Observation of first and second sound in a BKT superfluid

https://doi.org/10.1038/s41586-021-03537-9

Received: 24 August 2020

Accepted: 12 April 2021

Published online: 9 June 2021

Check for updates

Panagiotis Christodoulou[1]✉, Maciej Gałka[1], Nishant Dogra[1], Raphael Lopes[2], Julian Schmitt[1,3] & Zoran Hadzibabic[1]

Superfluidity in its various forms has been of interest since the observation of frictionless flow in liquid helium II[1,2]. In three spatial dimensions it is conceptually associated with the emergence of long-range order at a critical temperature. One of the hallmarks of superfluidity, as predicted by the two-fluid model[3,4] and observed in both liquid helium[5] and in ultracold atomic gases[6,7], is the existence of two kinds of sound excitation—the first and second sound. In two-dimensional systems, thermal fluctuations preclude long-range order[8,9]; however, superfluidity nevertheless emerges at a non-zero critical temperature through the infinite-order Berezinskii–Kosterlitz–Thouless (BKT) transition[10,11], which is associated with a universal jump[12] in the superfluid density without any discontinuities in the thermodynamic properties of the fluid. BKT superfluids are also predicted to support two sounds, but so far this has not been observed experimentally. Here we observe first and second sound in a homogeneous two-dimensional atomic Bose gas, and use the two temperature-dependent sound speeds to determine the superfluid density of the gas[13–16]. Our results agree with the predictions of BKT theory, including the prediction of a universal jump in the superfluid density at the critical temperature.

The hydrodynamic two-fluid theory[4] models a fluid below the critical temperature, T_c, as a mixture of a superfluid component and a viscous normal component that carries all the entropy, and assumes that the two are in local thermodynamic equilibrium. The two sounds then correspond to different variations of the total density and the entropy per particle. In three dimensions in the nearly incompressible liquid helium, the higher-speed first sound is a pure density wave and the lower-speed second sound is a pure entropy wave; more generally, both sounds can involve variations in both density and entropy[17]. At temperatures greater than T_c, the normal fluid supports just the first-sound density wave, and so the appearance of the second sound mode is a clear manifestation of superfluidity.

The two-sound phenomenology is also expected to hold for two-dimensional superfluids, despite the unconventional nature of the infinite-order BKT phase transition. However, in liquid-helium films, in which the BKT transition was first observed[18], the propagation of both first and second sound is inhibited because the viscous normal component is pinned by the substrate. In two-dimensional atomic gases, in which many complementary BKT experiments have been performed[19–31], only one sound mode has been seen so far. In a weakly interacting Bose gas, collisionless sound was observed[31–33] (see also ref. [34]) and showed no discontinuity at T_c, whereas in a strongly interacting Fermi gas, one pure density mode was observed[35] at temperatures well below T_c.

Here we observe both first and second sound in the long-wavelength density response of a homogeneous two-dimensional Bose gas to an external driving force (Fig. 1a). In our ^{39}K gas, which has a surface density $n \approx 3\,\mu m^{-2}$ and is characterized by a dimensionless interaction strength[24,36] $\tilde{g} = 0.64(3)$ (all uncertainties correspond to one standard deviation), the elastic collision rate is sufficiently high for collisional hydrodynamic behaviour. Specifically, near T_c it is about four times larger than the observed first-sound (angular) frequency ω_1; for comparison, in the experiment of ref. [31], for an ^{87}Rb gas with a similar geometry and larger n (~50 μm^{-2}) but smaller $\tilde{g}$ (0.16), the elastic collision rate and the expected[16] ω_1 were approximately equal near the critical point. At the same time, the compressibility of our gas near T_c is sufficiently high for our driving force to excite both sounds effectively[16,17].

Our homogeneous two-dimensional gases are prepared in a node of a vertical one-dimensional optical lattice (Fig. 1b, green) with harmonic trap frequency $\omega_z/(2\pi) = 5.5(1)$ kHz. They are deep in the two-dimensional regime; both the interaction and thermal energy per particle are below $0.3\hbar\omega_z$, where $\hbar$ is the reduced Planck's constant. In the x–y plane, we confine the atoms to a rectangular box of size $L_x \times L_y$ and potential-energy wall height U_0 using a hollow laser beam (Fig. 1b, red); we tune U_0/k_B, where k_B is the Boltzmann constant, to between 100 and 300 nK to vary the gas temperature T (Methods). We control the interaction strength $\tilde{g} = \sqrt{8\pi m\omega_z/\hbar}\,a$, where m is the atom mass and a the scattering length[24], via a magnetic Feshbach resonance[37] at 402.7 G. Our value of $\tilde{g}$ corresponds to a relatively high $a = 522(23)a_0$, where a_0 is the Bohr radius, which results in noticeable three-body losses; during the measurements (such as those in Fig. 1c) the sample slowly decays (without heating), but n stays within 15% of its average value and the data are fitted well by assuming a steady-state oscillation.

[1]Cavendish Laboratory, University of Cambridge, Cambridge, UK. [2]Laboratoire Kastler Brossel, Collège de France, CNRS, ENS-PSL Research University, Sorbonne Université, Paris, France. [3]Present address: Institut für Angewandte Physik, Universität Bonn, Bonn, Germany. ✉e-mail: pc558@cam.ac.uk

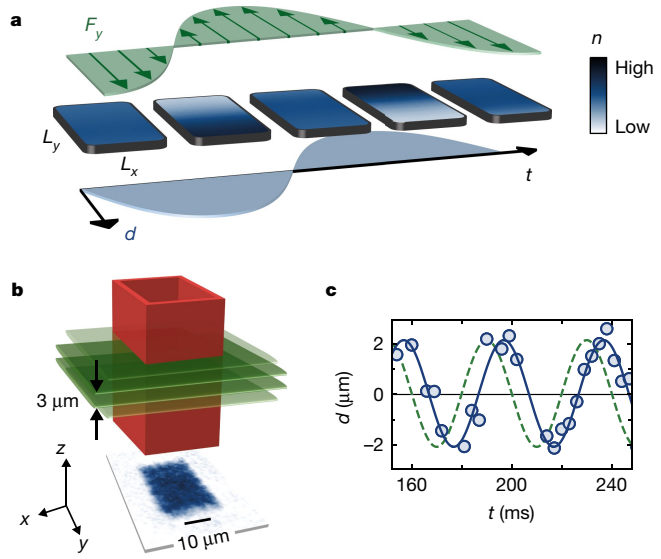

Fig. 1 | Sound excitations in a homogeneous two-dimensional Bose gas. **a**, An in-plane, spatially-uniform force $F_y(t) = F_0 \sin(\omega t)$, created by a magnetic field gradient, is applied on a homogeneous optically trapped two-dimensional gas. This excites long-wavelength density modulations with wavevector $q = \pi/L_y$, which results in a displacement of the cloud's centre of mass, $d(t)$. On resonance, d oscillates $\pi/2$ out of phase from F_y. **b**, Top, outline of the trapping setup; bottom, an absorption image of the two-dimensional gas. **c**, An example of $d(t)$ oscillation, for a gas below T_c and $\omega/(2\pi) = 25$ Hz near the second-sound resonance; for comparison, $L_y \approx 33$ μm. The green dashed curve indicates the phase of $F_y(t)$.

The driving force $F_y = F_0 \sin(\omega t)$ is aligned along the y direction, spatially uniform, and oscillating sinusoidally in time, t. It excites the longest-wavelength sound mode(s)[38], with wavevector $q = \pi/L_y$. The resulting density perturbation $\delta n(y, t)$ is proportional to $\sin(\pi y/L_y)$, with $y = 0$ in the box centre, and we define its oscillating amplitude $b(t)$ such that $\delta n(y, t)/n = b(t) \sin(\pi y/L_y)$. The corresponding displacement of the centre of mass of the cloud is then $d(t) = 2b(t)L_y/\pi^2$. We choose the driving-force amplitude F_0 so that even for resonant ω the maximal $d(t)$ is a few per cent of L_y (Fig. 1c) and fit $d(t) = R(\omega)\sin(\omega t) - A(\omega)\cos(\omega t)$, which gives the reactive (R) and absorptive (A) response.

We focus on $A(\omega)$, which is proportional to the imaginary part of the density response function (Methods) and reveals the phase transition. From energy conservation, namely the equality of the excitation energy and the energy pumped into the system, it follows that the response spectrum $A(\omega)$ must satisfy the f sum rule[39]

$$f_{\mathrm{sum}} = \int_{-\infty}^{\infty} \mathrm{d}\omega\, \omega \frac{\pi A(\omega)}{8F_0/m} = 1\,, \qquad (1)$$

with different excitation modes contributing to f_{sum} according to their oscillator strengths. Experimentally verifying that $f_{\mathrm{sum}} = 1$ ensures that all modes have been observed. In our case, below T_c the excitation spectrum should consist of first and second sound, with contributions f_1 and f_2, respectively, to f_{sum}. Above T_c the second-sound mode vanishes and a diffusive heat mode should appear; this mode also couples to the density and contributes f_{diff} to f_{sum} (Methods). From $A(\omega)$ we also obtain the dynamical structure factor[17] $S(q, \omega) = \pi q^2 k_B T A(\omega)/(8\omega F_0)$, which reveals the qualitative difference between propagating sound modes and the diffusive mode[40,41]—for the former, $S(\omega)$ has a maximum at non-zero ω, whereas for the latter, the maximum occurs at $\omega = 0$.

Figure 2a, b shows the different responses of the system below and above the critical temperature. Here we express all results in dimensionless form, using the Bogoliubov frequency $\omega_B = c_B q$, where $c_B = \hbar\sqrt{n\tilde{g}}/m \approx 2.3$ mm s^{-1} is the Bogoliubov sound speed. Specifically, we define $\tilde{A} = \pi m \omega_B^2 A/(8F_0)$, so $f_{\mathrm{sum}} = \int \mathrm{d}\omega\, \omega \tilde{A}/\omega_B^2$ and $S = k_B T \tilde{A}/(m c_B^2 \omega)$; for the fitting procedure, see Methods. In Fig. 2a, the two resolved resonances observed below T_c correspond to the first and second sound, and the resonance frequencies ω_1 and $\omega_2 < \omega_1$ give the sound speeds $c_{1,2} = \omega_{1,2}/q$. Above T_c, the sole resonance is attributed to the first sound, whereas the low-frequency 'shoulder' is attributed to the diffusive mode that replaces the second sound. Figure 2b shows the corresponding $S(\omega)$, and the inset highlights the difference between second sound ($c_2 > 0$) and the diffusive mode corresponding to $c_2 = 0$. The width of the diffusive mode gives the thermal diffusivity $D_T = 5(2)\hbar/m$. With a caveat that our sound resonances might be broadened by the loss-induced density drift, their widths imply sound diffusivities $D_{s,1} = 7(1)\hbar/m$ and

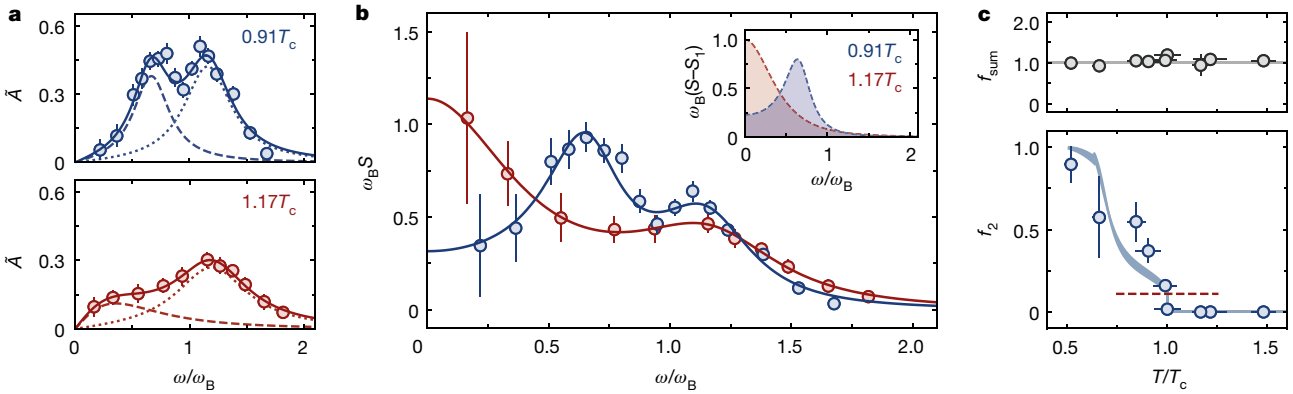

Fig. 2 | First and second sound. a, Normalized response spectra $\tilde{A}(\omega)$ at $0.91T_c$ and $1.17T_c$ for $n \approx 3$ μm^{-2}, $L_y \approx 33$ μm and $F_0/m \approx 0.074$ m s^{-2}. Below T_c (top) we observe two resonances corresponding to the first (dotted) and second (dashed) sound. Above T_c (bottom) we instead observe just the first-sound resonance (dotted), while the second sound is replaced by a diffusive, overdamped mode (dashed). **b**, The corresponding dynamical structure factors $S(\omega)$. Here the diffusive mode has a maximum at $\omega = 0$, so its distinction from the second-sound resonance is clearer. The inset shows the fitted contributions to $S(\omega)$ from the second sound below T_c (blue) and the diffusive mode above T_c (red), omitting for clarity the first-sound contributions $S_1(\omega)$, which are similar at the two temperatures. **c**, The f sum rule and the critical point. Top, the f sum rule is verified over a wide range of temperatures. Bottom, f_2, the second-sound contribution to the constant f_{sum}, vanishes with increasing T and is used to experimentally identify T_c. The blue shading shows the theoretical prediction for an infinite dissipationless system, with no free parameters. The thickness of the shaded area reflects the theoretical variations due to the uncertainty in $\tilde{g}$. The dashed line indicates the predicted discontinuity in f_2 at T_c, which arises from the jump in the superfluid density. The error bars in all panels show standard fitting errors.

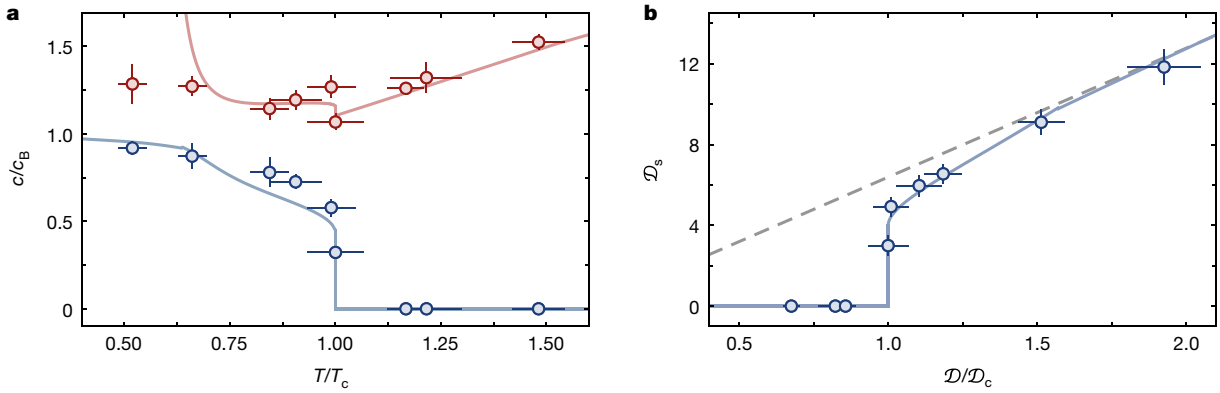

Fig. 3 | The sound speeds and the superfluid density. a, Normalized sound speeds, c_1/c_B (red) and c_2/c_B (blue), and the corresponding theoretical predictions without any free parameters. Owing to scale invariance in two dimensions, the predicted $c_{1,2}/c_B$ are functions of just T/T_c and $\tilde{g}$. Their discontinuities at T_c correspond to the infinite-system jump in superfluid density. **b**, The superfluid phase-space density, $\mathcal{D}_s$, deduced using the measured sound speeds. The solid line, showing the universal jump of $\mathcal{D}_s$ from 0 to 4 at $\mathcal{D} = \mathcal{D}_c$, is the infinite-system theoretical prediction without any free parameters. The dashed line corresponds to a 100% superfluid ($\mathcal{D}_s = \mathcal{D}$). All error bars show standard statistical errors.

$10(2)\hbar/m$ for the first sound below and above T_c, respectively, and $D_{s,2} = 6(1)\hbar/m$ for the second sound below T_c. For comparison, sound diffusivities that are several times lower, at approximately $\hbar/m$, were observed in strongly interacting two-dimensional[35] and three-dimensional[42] Fermi gases.

In Fig. 2c we plot the fitted f_{sum} for a range of temperatures, showing that it always satisfies the f sum rule. We also show how f_2 vanishes with increasing T, a finding that we used to experimentally identify T_c. In absolute terms, including our systematic uncertainties in n and T (Methods), $T_c = 42(4)$ nK for $n = 3.0(5)\ \mu m^{-2}$, which is compatible with the BKT prediction[13] $T_c = 2\pi n\hbar^2/[mk_B \ln(380/\tilde{g})] = 37(6)$ nK. In a finite-size system the transition is rounded-off into a crossover[19,43–45] (see also refs. [18,34] for non-zero-ω effects), and for our system parameters this could indeed increase T_c by approximately 10%; however, within our errors this shift is not conclusive.

Figure 3a displays the temperature-dependent speeds of the first and second sound, normalized to c_B. The solid lines represent values predicted according to infinite-system theory[15,16] without any free parameters, and are generally in good agreement with the data. Crucially, these theoretical results rely on both thermodynamic calculations and the predictions of the superfluid density[11,12,14]. The relevant thermodynamic calculations were performed in ref. [14] assuming $\tilde{g} \ll 1$; however, previous experiments have verified their applicability for a wide range of interaction strengths[22,23,26], including the one used in this work. Regarding the superfluid density n_s, a key prediction of the infinite-system BKT theory is that it exhibits a jump[12] at T_c from 0 to $4/\lambda^2$, where λ is the thermal wavelength. For our value of $\tilde{g}$, the most pronounced effect of this jump is a discontinuity in c_2 of about $0.45c_B$, with less pronounced discontinuities in c_1 and f_2 (see Fig. 2c)[15]. For our data at $T/T_c < 0.75$, where the expected superfluid fraction is close to 100% and $c_2 \approx c_B$, the predictions for c_1 are not reliable because they are very sensitive to the exact value of the vanishingly small normal-component density[16].

Finally, instead of comparing the measured and predicted sound speeds, we can combine our measurements of $c_{1,2}$ and the previously verified[22,23,26] thermodynamic calculations[14] to deduce n_s and compare it directly with theory[12,14] (Methods); a similar procedure was previously used for a strongly interacting three-dimensional Fermi superfluid[7]. In Fig. 3b, we plot the deduced superfluid phase-space density $\mathcal{D}_s = n_s\lambda^2$ versus $\mathcal{D}/\mathcal{D}_c$, where $\mathcal{D} = n\lambda^2$ is the total phase-space density and $\mathcal{D}_c$ is its critical value. The solid line is the theoretical prediction[14] without any free parameters, which shows the universal, $\tilde{g}$-independent jump of $\mathcal{D}_s$ from 0 to 4 at the critical point.

Our experiments establish the applicability of the two-fluid model to unconventional BKT superfluids. We provide the first—to our knowledge—measurement of the superfluid density in an atomic two-dimensional gas, and experimentally demonstrate the predicted universal jump at the critical point. Our measurements also extend into the low-temperature regime, in which a complete theoretical picture is not yet available. An experimental challenge for future work is to explore even lower temperatures, at which hybridization of the first and second sound is expected[46,47]. More generally, establishing measurements of the superfluid density in two-dimensional quantum gases provides an invaluable diagnostic tool for many future studies, including exploration of non-equilibrium phenomena and of the effects of disorder on superfluidity.

Online content

Any methods, additional references, Nature Research reporting summaries, source data, extended data, supplementary information, acknowledgements, peer review information; details of author contributions and competing interests; and statements of data and code availability are available at https://doi.org/10.1038/s41586-021-03537-9.

1. Kapitza, P. Viscosity of liquid helium below the λ-point. *Nature* **141**, 74 (1938).
2. Allen, J. F. & Misener, A. D. Flow of liquid helium II. *Nature* **141**, 75 (1938).
3. Tisza, L. Transport phenomena in helium II. *Nature* **141**, 913 (1938).
4. Landau, L. Theory of the superfluidity of helium II. *Phys. Rev.* **60**, 356–358 (1941).
5. Peshkov, V. Second sound in helium II. *Sov. Phys. JETP* **11**, 580–584 (1960).
6. Stamper-Kurn, D. M., Miesner, H.-J., Inouye, S. & Andrews, M. R. & Ketterle, W. Collisionless and hydrodynamic excitations of a Bose–Einstein condensate. *Phys. Rev. Lett.* **81**, 500–503 (1998).
7. Sidorenkov, L. A. et al. Second sound and the superfluid fraction in a Fermi gas with resonant interactions. *Nature* **498**, 78–81 (2013).
8. Hohenberg, P. C. Existence of long-range order in one and two dimensions. *Phys. Rev.* **158**, 383–386 (1967).
9. Mermin, N. D. & Wagner, H. Absence of ferromagnetism or antiferromagnetism in one- or two-dimensional isotropic Heisenberg models. *Phys. Rev. Lett.* **17**, 1307 (1966).
10. Berezinskii, V. L. Destruction of long-range order in one-dimensional and two-dimensional systems possessing a continous symmetry group. II. Quantum systems. *Sov. Phys. JETP* **34**, 610 (1971).
11. Kosterlitz, J. M. & Thouless, D. J. Ordering, metastability and phase transitions in twodimensional systems. *J. Phys. C* **6**, 1181–1203 (1973).
12. Nelson, D. R. & Kosterlitz, J. M. Universal jump in the superfluid density of two-dimensional superfluids. *Phys. Rev. Lett.* **39**, 1201–1205 (1977).
13. Prokof'ev, N., Ruebenacker, O. & Svistunov, B. Critical point of a weakly interacting two-dimensional Bose gas. *Phys. Rev. Lett.* **87**, 270402 (2001).
14. Prokof'ev, N. & Svistunov, B. Two-dimensional weakly interacting Bose gas in the fluctuation region. *Phys. Rev. A* **66**, 043608 (2002).
15. Ozawa, T. & Stringari, S. Discontinuities in the first and second sound velocities at the Berezinskii–Kosterlitz–Thouless transition. *Phys. Rev. Lett.* **112**, 025302 (2014).
16. Ota, M. & Stringari, S. Second sound in a two-dimensional Bose gas: from the weakly to the strongly interacting regime. *Phys. Rev. A* **97**, 033604 (2018).
17. Hu, H., Taylor, E., Liu, X.-J., Stringari, S. & Griffin, A. Second sound and the density response function in uniform superfluid atomic gases. *New J. Phys.* **12**, 043040 (2010).

18. Bishop, D. J. & Reppy, J. D. Study of the superfluid transition in two-dimensional ^{4}He films. *Phys. Rev. Lett.* **40**, 1727–1730 (1978).
19. Hadzibabic, Z., Krüger, P., Cheneau, M., Battelier, B. & Dalibard, J. Berezinskii–Kosterlitz–Thouless crossover in a trapped atomic gas. *Nature* **441**, 1118–1121 (2006).
20. Cladé, P., Ryu, C., Ramanathan, A., Helmerson, K. & Phillips, W. D. Observation of a 2D Bose gas: from thermal to quasicondensate to superfluid. *Phys. Rev. Lett.* **102**, 170401 (2009).
21. Tung, S., Lamporesi, G., Lobser, D., Xia, L. & Cornell, E. A. Observation of the presuperfluid regime in a two-dimensional Bose gas. *Phys. Rev. Lett.* **105**, 230408 (2010).
22. Yefsah, T., Desbuquois, R., Chomaz, L., Günter, K. J. & Dalibard, J. Exploring the thermodynamics of a two-dimensional Bose gas. *Phys. Rev. Lett.* **107**, 130401 (2011).
23. Hung, C.-L., Zhang, X., Gemelke, N. & Chin, C. Observation of scale invariance and universality in two-dimensional Bose gases. *Nature* **470**, 236–239 (2011).
24. Hadzibabic, Z. & Dalibard, J. Two-dimensional Bose fluids: an atomic physics perspective. *Riv. Nuovo Cimento* **34**, 389–434 (2011).
25. Desbuquois, R. et al. Superfluid behaviour of a two-dimensional Bose gas. *Nat. Phys.* **8**, 645–648 (2012).
26. Ha, L.-C. et al. Strongly interacting two-dimensional Bose gases. *Phys. Rev. Lett.* **110**, 145302 (2013).
27. Choi, J. Y., Seo, S. W. & Shin, Y. I. Observation of thermally activated vortex pairs in a quasi-2D Bose gas. *Phys. Rev. Lett.* **110**, 175302 (2013).
28. Chomaz, L. et al. Emergence of coherence via transverse condensation in a uniform quasi-two-dimensional Bose gas. *Nat. Commun.* **6**, 6162 (2015).
29. Fletcher, R. J. et al. Connecting Berezinskii–Kosterlitz–Thouless and BEC phase transitions by tuning interactions in a trapped gas. *Phys. Rev. Lett.* **114**, 255302 (2015).
30. Murthy, P. A. et al. Observation of the Berezinskii–Kosterlitz–Thouless phase transition in an ultracold Fermi gas. *Phys. Rev. Lett.* **115**, 010401 (2015).
31. Ville, J. L. et al. Sound propagation in a uniform superfluid two-dimensional Bose gas. *Phys. Rev. Lett.* **121**, 145301 (2018).
32. Ota, M. et al. Collisionless sound in a uniform two-dimensional Bose gas. *Phys. Rev. Lett.* **121**, 145302 (2018).
33. Cappellaro, A., Toigo, F. & Salasnich, L. Collisionless dynamics in two-dimensional bosonic gases. *Phys. Rev. A* **98**, 043605 (2018).
34. Wu, Z., Zhang, S. & Zhai, H. Dynamic Kosterlitz–Thouless theory for two-dimensional ultracold atomic gases. *Phys. Rev. A* **102**, 043311 (2020).
35. Bohlen, M. et al. Sound propagation and quantum-limited damping in a two-dimensional Fermi gas. *Phys. Rev. Lett.* **124**, 240403 (2020).
36. Petrov, D. S., Holzmann, M. & Shlyapnikov, G. V. Bose–Einstein condensation in quasi-2D trapped gases. *Phys. Rev. Lett.* **84**, 2551–2555 (2000).
37. Fletcher, R. J. et al. Elliptic flow in a strongly interacting normal Bose gas. *Phys. Rev. A* **98**, 011601 (2018).
38. Navon, N., Gaunt, A. L., Smith, R. P. & Hadzibabic, Z. Emergence of a turbulent cascade in a quantum gas. *Nature* **539**, 72–75 (2016).
39. Pitaevskii, L. & Stringari, S. *Bose–Einstein Condensation and Superfluidity* Ch. 7 (Oxford Univ. Press, 2016).
40. Hohenberg, P. C. & Martin, P. C. Superfluid dynamics in the hydrodynamic ($\omega\tau \ll 1$) and collisionless ($\omega\tau \gg 1$) domains. *Phys. Rev. Lett.* **12**, 69–71(1964).
41. Singh, V. P. & Mathey, L. Sound propagation in a two-dimensional Bose gas across the superfluid transition. *Phys. Rev. Res.* **2**, 023336 (2020).
42. Patel, P. B. et al. Universal sound diffusion in a strongly interacting Fermi gas. *Science* **370**, 1222–1226 (2020).
43. Pilati, S., Giorgini, S. & Prokof'ev, N. Critical temperature of interacting Bose gases in two and three dimensions. *Phys. Rev. Lett.* **100**, 140405 (2008).
44. Foster, C. J., Blakie, P. B. & Davis, M. J. Vortex pairing in two-dimensional Bose gases. *Phys. Rev. A* **81**, 023623 (2010).
45. Gawryluk, K. & Brewczyk, M. Signatures of a universal jump in the superfluid density of a two-dimensional Bose gas with a finite number of particles. *Phys. Rev. A* **99**, 033615 (2019).
46. Lee, T. D. & Yang, C. N. Low-temperature behavior of a dilute Bose system of hard spheres. II. Nonequilibrium properties. *Phys. Rev.* **113**, 1406–1413 (1959).
47. Pitaevskii, L. & Stringari, S. In *Universal Themes of Bose-Einstein Condensation* (eds Proukakis, N. P. et al.) 322–347 (Cambridge Univ. Press, 2017).

Methods

Optical confinement of the two-dimensional gas

The one-dimensional optical lattice and the rectangular hollow beam are blue-detuned from the atomic resonance, and create repulsive potentials for the atoms. Both are shaped using digital micromirror devices (DMDs). The hollow beam providing the in-plane confinement has a wavelength of 760 nm and is created by direct imaging of a DMD pattern. The vertical one-dimensional lattice is made of 532-nm light and is created by Fourier imaging of a DMD pattern, which allows dynamical tuning of the lattice period Δz. Specifically, using a DMD we create two horizontal light strips, each of width corresponding to 50 micromirror pixels, separated vertically by ΔZ, so their interference in the Fourier plane creates a lattice with $\Delta z \propto 1/\Delta Z$. We additionally impose a phase shift of π between the two interfering beams, which places the central node of the symmetric interference pattern at $z = 0$ independently of the varying Δz. To dynamically change Δz we shift the DMD pattern pixel by pixel (moving the two light strips symmetrically in opposite directions) in 25-ms steps. We start with a large $\Delta z = 18.5$ μm to load a three-dimensional gas, pre-cooled as in ref. [48], into a single lattice node. We then reduce Δz over a period of 1.5 s to 3.3 μm in order to compress the gas into the two-dimensional geometry. In the final two-dimensional configuration, the lattice depth around the central node is $U_z \approx 3.0$ μK, giving the trap frequency $\omega_z/(2\pi) = (\Delta z)^{-1}\sqrt{U_z/(2m)} = 5.5$ kHz.

Calibration of the experimental parameters

Our absorption imaging system, used to measure the cloud density n, is calibrated with a systematic uncertainty of 15% using measurements of the critical temperature for Bose–Einstein condensation in a three-dimensional harmonic trap[49]; this calibration also agrees with an independent one that is based on the rates of the density-dependent three-body decay[50]. We assess the absolute gas temperature with a systematic uncertainty of 10% using measurements of the scale-invariant two-dimensional equation of state[14,22,23,26], as in ref. [31]; we have made equation of state measurements for several trap depths U_0 and also different trap dimensions L_x and L_y, which show linear dependence of T on U_0. The wavevector $q = \pi/L_y$ is determined using in situ absorption images (such as the one shown in Fig. 1b), with a systematic 5% error due to the fact that the cloud edges are not infinitely sharp; the half-wavelength of the density modulation closely corresponds to the length of the region in which the density is greater than 90% of its value in the bulk. The driving-force amplitude F_0 is calibrated with an error of 5% by applying a constant force on a cloud released from the trap and measuring the resulting centre-of-mass acceleration.

Response function, *f* sum rule and $S(\omega)$

The density response function is defined in Fourier space as $\chi_{nn}(q,\omega) = \delta n(q,\omega)/\delta U(q,\omega)$, where $\delta U(q,\omega)$ is the driving potential. Our monochromatic and spatially uniform driving force corresponds to a potential $-F_0 y \sin(\omega t)$ for $-L_y/2 \le y \le L_y/2$, and Fourier decomposition of this gives $\delta U(q = \pi/L_y, \omega) = -4F_0L_y/\pi^2$. Following our definition of $A(\omega)$ gives $\mathrm{Im}[\chi_{nn}(q = \pi/L_y, \omega)] = -\pi^2 nq^2 A(\omega)/(8F_0)$. Inserting this into the conventional form of the *f* sum rule[39],

$$\int_{-\infty}^{\infty} \mathrm{d}\omega\, \omega\, \mathrm{Im}[\chi_{nn}(q,\omega)] = -\frac{\pi n q^2}{m}, \qquad (2)$$

gives the dimensionless sum rule in equation (1), which is insensitive to uncertainties and variations in n and q. Our dimensionless results in Fig. 2c (and also Fig. 3) are also not affected by changes in F_0; for these measurements we have varied F_0 by a factor of 3. We have also varied q by about 50%, by using two different box sizes of $(L_x, L_y) \approx$ (21 μm, 33 μm) and (56 μm, 23 μm). The dynamical structure factor is (for $k_B T \gg \hbar\omega$, which is always satisfied in our experiments) given by $S(q,\omega) = -k_B T\, \mathrm{Im}[\chi_{nn}(q,\omega)]/(\pi n\omega)$, which is equivalent to the form given in the text in terms of $A(\omega)$.

Fits of the response spectra

In the two-fluid model, ignoring dissipation, the density response function is[17]

$$\chi_{nn}(q,\omega) = \frac{nq^2}{m}\left(\frac{Z_1}{\omega^2 - c_1^2 q^2} + \frac{Z_2}{\omega^2 - c_2^2 q^2}\right), \qquad (3)$$

with the two poles giving the sound speeds $c_{1,2}$, and $Z_1 + Z_2 = 1$ to satisfy the *f* sum rule. Including linear damping[51], we fit the experimental spectra with $A(\omega) = A_1(\omega) + A_2(\omega)$, where

$$A_{1,2}(\omega) = \frac{x_{1,2}\omega_{1,2}^2 \Gamma_{1,2}\omega}{(\omega^2 - \omega_{1,2}^2)^2 + (\omega\Gamma_{1,2})^2}. \qquad (4)$$

Here the amplitudes $x_{1,2}$, resonance frequencies $\omega_{1,2}$ (with $\omega_1 > \omega_2$) and damping rates $\Gamma_{1,2}$, are fit parameters, and the sound diffusivities are then given by $\Gamma_{1,2}/q^2$. For consistency, we first apply the same fit to the data taken at all temperatures, and find that it always captures the data well and gives $f_{sum} \approx 1$ (Fig. 2c). The first sound is always underdamped and the A_1 term gives f_1, its contribution to f_{sum}. For the spectra identified as being below T_c (as in the top panel of Fig. 2a), the fit gives that the second sound is also underdamped, and its contribution to $S(\omega)$ peaks at a non-zero ω. In this case A_2 gives the non-zero f_2 contribution to f_{sum}. For the data identified as being above T_c (as in the bottom panel of Fig. 2a), the second term in the fit function shows that this mode is overdamped, and its contribution to $S(\omega)$ peaks at $\omega = 0$. This demonstrates, in an unbiased way, that the second sound is replaced by the diffusive mode. In this case the A_2 term gives f_{diff}, the diffusive-mode contribution to f_{sum}, with $f_1 + f_{diff} \approx 1$, while $f_2 = 0$. Note that approximating the diffusive mode by a δ-function response[17] at $\omega = 0$ gives $f_{diff} = 0$, but in reality this mode has a non-zero contribution to the experimental f_{sum} shown in Fig. 2c (top). To quantitatively assess the thermal diffusivity D_T, following refs. [51,52] we refit the data for $T > T_c$ with $A(\omega) = A_1(\omega) + A_T(\omega)$, where

$$A_T(\omega) = \frac{x_T \Gamma_T \omega}{\omega^2 + \Gamma_T^2} \qquad (5)$$

corresponds to a contribution to $S(\omega)$ that is a Lorentzian centred at $\omega = 0$, and gives $D_T = \Gamma_T/q^2$.

Sound speeds and the superfluid density

The theoretical predictions for the two sound speeds, c_1 and c_2, are the solutions of the quartic equation for c:

$$c^4 - (c_{10}^2 + c_{20}^2)c^2 + c_{10}^2 c_{20}^2/\gamma = 0, \qquad (6)$$

where $c_{10}^2 = 1/(mn\kappa_S)$ and $c_{20}^2 = Ts^2 n_s/[mc_V(n - n_s)]$; here c_V is the specific heat per particle at constant volume, s is the entropy per particle and $\gamma = \kappa_T/\kappa_S \ge 1$ is the ratio of the isothermal and isentropic compressibilites[17,51]. As detailed in equations (2) and (3) of ref. [15], all the relevant thermodynamic quantities are linked to the phase-space density calculated in ref. [14] and experimentally verified in refs. [22,23,26]. Crucially, in addition to these thermodynamic quantities, c_{20} explicitly depends on the superfluid density n_s. For $\gamma \to 1$, which is the case in nearly incompressible superfluids such as three-dimensional liquid helium and unitary Fermi gases, $c_1 \to c_{10}$ and $c_2 \to c_{20}$, so to a good approximation only c_2 depends on n_s. However, when γ is clearly distinct from 1, which is typically the case for a Bose gas near T_c, both sound speeds depend on n_s; for our value of $\tilde{g}$, we find $\gamma \approx 1.6$ at the critical temperature[16]. The theoretical speeds[14–16] in Fig. 3a are based on the previously verified thermodynamic predictions and the hitherto unverified predictions

for n_s. Conversely, we can use our measured c_1 and c_2 (for $T < T_c$), which together give c_{20}, and the established thermodynamic calculations to deduce n_s; this gives the results shown in Fig. 3b. Note that owing to the scale-invariance in two dimensions[22,23], for a given $\tilde{g}$ both the superfluid fraction and all the thermodynamic quantities depend only on T/T_c.

Data availability

The data that support the findings of this study are available in the Apollo repository (https://doi.org/10.17863/CAM.66056). Any additional information is available from the corresponding authors upon reasonable request. Source data are provided with this paper.

48. Eigen, C. et al. Observation of weak collapse in a Bose–Einstein condensate. *Phys. Rev. X* **6**, 041058 (2016).
49. Campbell, R. L. D. et al. Efficient production of large ^{39}K Bose–Einstein condensates. *Phys. Rev. A* **82**, 063611 (2010).
50. Zaccanti, M. et al. Observation of an Efimov spectrum in an atomic system. *Nat. Phys.* **5**, 586 (2009).
51. Hohenberg, P. C. & Martin, P. C. Microscopic theory of superfluid helium. *Ann. Phys.* **34**, 291 (1965).
52. Hu, H., Zou, P. & Liu, X.-J. Low-momentum dynamic structure factor of a strongly interacting Fermi gas at finite temperature: a two-fluid hydrodynamic description. *Phys. Rev. A* **97**, 023615 (2018).

Acknowledgements We thank J. Man for experimental assistance; and R. P. Smith, J. Dalibard, M. Zwierlein, R. J. Fletcher, T. A. Hilker, S. Nascimbene and T. Yefsah for discussions. This work was supported by the EPSRC (grant nos EP/N011759/1 and EP/P009565/1), ERC (QBox) and QuantERA (NAQUAS, EPSRC grant no. EP/R043396/1). J.S. acknowledges support from Churchill College (Cambridge), and Z.H. acknowledges support from the Royal Society Wolfson Fellowship.

Author contributions P.C. led the data acquisition and analysis. M.G. and J.S. contributed to the data acquisition. P.C., M.G., R.L. and J.S. contributed to the experimental setup. P.C., N.D. and J.S. produced the figures. Z.H. supervised the project. All authors contributed to the data analysis, interpretation of the results and writing of the manuscript.

Competing interests The authors declare no competing interests.

Additional information
Correspondence and requests for materials should be addressed to P.C.
Peer review information *Nature* thanks the anonymous reviewers for their contribution to the peer review of this work.
Reprints and permissions information is available at http://www.nature.com/reprints.